

DiffX: Guide Your Layout to Cross-Modal Generative Modeling

Zeyu Wang^{1*}, Jingyu Lin^{2*}, Yifei Qian³, Yi Huang⁴, Shicen Tian¹, Bosong Chai¹, Juncan Deng¹, Lan Du², Cunjian Chen², Yufei Guo^{4†}, Kejie Huang^{1†}

¹Zhejiang University, ²Monash University, ³University of Nottingham, ⁴Peking University

{wangzeyu2020, tianshichen, chaibosong, dengjuncan, huangkejie}@zju.edu.cn,

{jingyu.lin, lan.du, cunjian.chen}@monash.edu,

Yifei.Qian@nottingham.ac.uk, yihuang@stu.pku.edu.cn, yfguo@pku.edu.cn

Abstract

Diffusion models have made significant strides in language-driven and layout-driven image generation. However, most diffusion models are limited to visible RGB image generation. In fact, human perception of the world is enriched by diverse viewpoints, such as chromatic contrast, thermal illumination, and depth information. In this paper, we introduce a novel diffusion model for general layout-guided cross-modal generation, called DiffX. Notably, DiffX presents a simple yet effective cross-modal generative modeling pipeline, which conducts diffusion and denoising processes in the modality-shared latent space. Moreover, we introduce the Joint-Modality Embedder (JME) to enhance interaction between layout and text conditions by incorporating a gated attention mechanism. Meanwhile, the advanced Long-CLIP is employed for long caption embedding for user instruction. To facilitate the user-instructed generative training, we construct the cross-modal image datasets with detailed text captions assisted by the Large-Multimodal Model (LMM). Through extensive experiments, DiffX demonstrates robustness in cross-modal generation across three “RGB+X” datasets: FLIR, MFNet, and COME15K, guided by various layout conditions. It also shows the potential for the adaptive generation of “RGB+X+Y+Z” images or more diverse modalities on COME15K and MCXFace datasets. Our code and constructed cross-modal image datasets are available at <https://github.com/zeyuwang-zju/DiffX>.

1 Introduction

Over the past decade, there have been significant advancements in image generation, driven by the improvement of deep generative models such as Variational AutoEncoders (VAEs) (Kingma and Welling 2013) and Generative Adversarial Networks (GANs) (Goodfellow et al. 2014). Prominently, the recent diffusion models (Sohl-Dickstein et al. 2015; Ho, Jain, and Abbeel 2020) like DALL-E (Ramesh et al. 2021, 2022), Imagen (Saharia et al. 2022), and Stable Diffusion (SD) (Rombach et al. 2022) have gained great popularity for their ability to generate high-fidelity images conditioned on text descriptions or class labels. Moreover, the field has witnessed the rise of layout-to-image models based on various layout conditions, including bounding boxes, semantic maps, and keypoints (Xie et al. 2023; Li

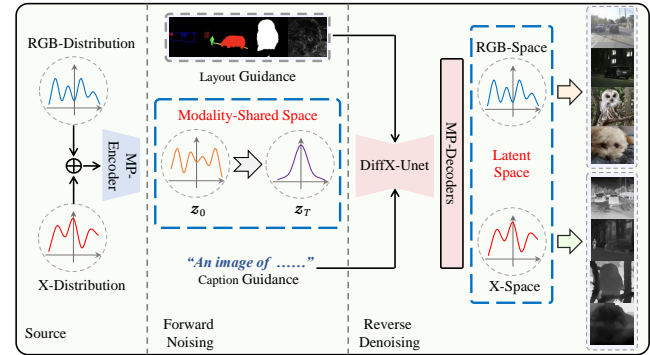


Figure 1: Cross-modal generative pipeline in latent space.

et al. 2023; Ma et al. 2024). The success of diffusion models can be attributed to their stable learning objective and the availability of large-scale multi-modal training data.

Current layout-to-image diffusion models primarily focus on generating high-quality visible RGB images. However, our perception of the world is enhanced by a multitude of perspectives beyond the visible spectrum, including thermal imaging, depth perception, and so on. Cross-modal visual understanding typically leverages the input format of “RGB+X”, where X represents additional data like Thermal (T) or Depth (D) images. It offers a more comprehensive representation compared with RGB-only understanding, especially in challenging environments. At present, a significant limitation lies in the scarcity of cross-modal data containing pixel-aligned RGB+X image pairs. If the conventional generative models are adopted for cross-modal data augmentation, we can only generate RGB and X images separately, and as a result, the RGB and X images cannot form consistent pairs of matching data. Consequently, we wonder *if we can generate the cross-modal images simultaneously under layout guidance by an integrated model?*

In this work, we introduce a novel diffusion model for cross-modal image generation, called DiffX. As shown in Figure 1, our proposed DiffX model is capable of generating RGB+X image pairs and more diverse modalities guided by various layouts. Our main contributions are as follows:

- We propose an effective cross-modal generative modeling pipeline, which performs the diffusion and denoising

*These authors contributed equally.

†Corresponding authors.

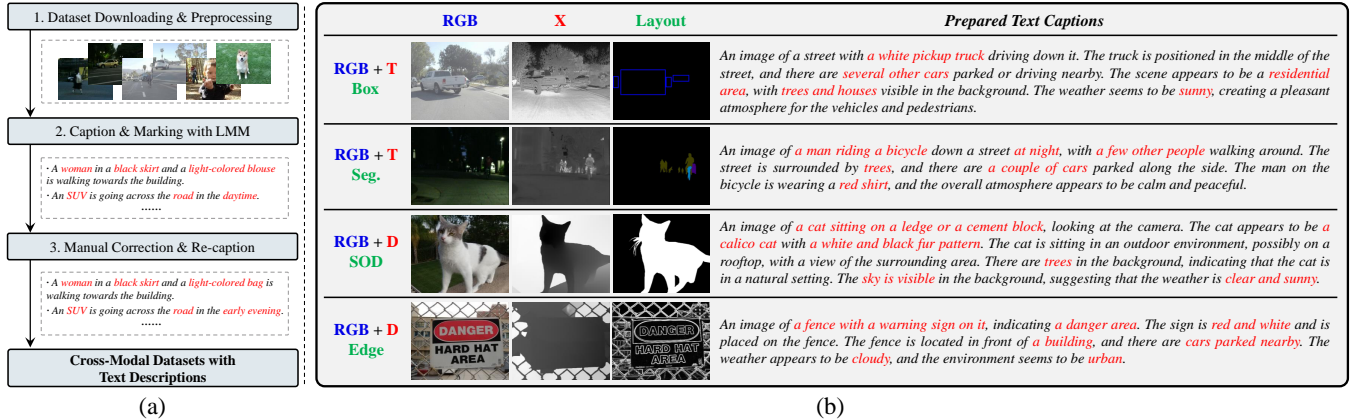


Figure 2: (a) The process of constructing the image captions. (b) Examples of cross-modal images, labels, and prepared captions.

processes in modality-shared latent space, facilitated by our Multi-Path Variational AutoEncoder (MP-VAE).

- We propose a Joint-Modality Embedder (JME) to establish the connection between layout and text conditions via the gated cross-attention mechanism. Besides, we employ the advanced Long-CLIP (Zhang et al. 2024) to capture critical information in cross-modal captions.
- Due to the limited cross-modal data with text descriptions, we leverage a Large-Multimodal Model (LMM) to construct captions, followed by manual corrections.
- Our experiments demonstrate that DiffX can generate high-quality and coherent “RGB+X” image pairs based on bounding boxes, semantic maps, salient maps, and edges. Additionally, it demonstrates strong adaptability to “RGB+X+Y+Z” or diverse-modal generation.

2 Related Works

2.1 Cross-Modal Visual Understanding

Cross-modal visual understanding normally adopts RGB+X input data. Thermal images have shown advantages in detecting objects in low-light conditions. For instance, CFT (Fang, Han, and Wang 2021) and ICAFusion (Shen et al. 2024) incorporate Transformer-based RGB+T feature fusion modules for multispectral object detection. In semantic segmentation, EGFNet (Zhou et al. 2022) leverages prior edge maps of RGB+T images to capture detailed contour information. Meanwhile, depth images exhibit valuable insights into spatial structures and 3D layouts. For example, HidaNet (Wu et al. 2023) utilizes a granularity-based attention mechanism to enhance the advantages of RGB+D features for Salient Object Detection (SOD). However, current cross-modal visual understanding is hindered by the lack of well-aligned RGB+X image pairs for training deep models.

2.2 Layout-to-Image Generation

Based on Denoising Diffusion Probabilistic Model (DDPM) (Sohl-Dickstein et al. 2015; Ho, Jain, and Abbeel 2020), diffusion models have undergone advancements in training and sampling techniques (Song, Meng, and Ermon 2021; Nichol

and Dhariwal 2021). Recent studies have proposed layout-to-image diffusion models, which provide precise instructions for object generation. For example, LAW-Diffusion (Yang et al. 2023) integrates a spatial parser and adaptive guidance, enabling complex scene generation. BoxDiff (Xie et al. 2023) directly incorporates spatial conditions into the training-free denoising process. Additionally, InstanceDiffusion (Wang et al. 2024) focuses on precise instance-level control in high-quality image generation.

2.3 Multi-Modal Generation

Multi-modal generation has become a challenging task and attracted widespread research. MM-Diffusion (Ruan et al. 2023) integrates featuring two interconnected denoising autoencoders and a sequential multi-modal U-Net architecture for joint audio-video generation. Moreover, MM-Interleaved (Tian et al. 2024) dynamically extracts information from multi-scale features for image-text generation. In addition, ControlVAR (Li et al. 2024), MT-Diffusion (Chen et al. 2024), and 4M (Mizrahi et al. 2024) adopt large-scale natural datasets or private datasets for end-to-end training on conditional generation. Despite these advancements, there is currently no generative model focused on layout-guided cross-modal “RGB+X(+Y)” image generation.

3 Cross-Modal Dataset Construction

Since DiffX aims to sample cross-modal images under user instruction, it is crucial to construct datasets with accurate layout control and text descriptions for model training. However, existing cross-modal datasets usually lack detailed text captions. In this section, we introduce the process of constructing the image captions, as illustrated in Figure 2 (a).

Caption Generation: To obtain high-quality image captions, we employ the advanced LMM, namely LLaVA-v1.5-7b model (Liu et al. 2024), to extract detailed descriptions of the images by the given prompt, including weather conditions, environmental settings, surrounding elements, transportation conditions, and identifiable objects.

Caption Correction: Despite the effectiveness of LLaVA in capturing visual content, it can sometimes generate inac-

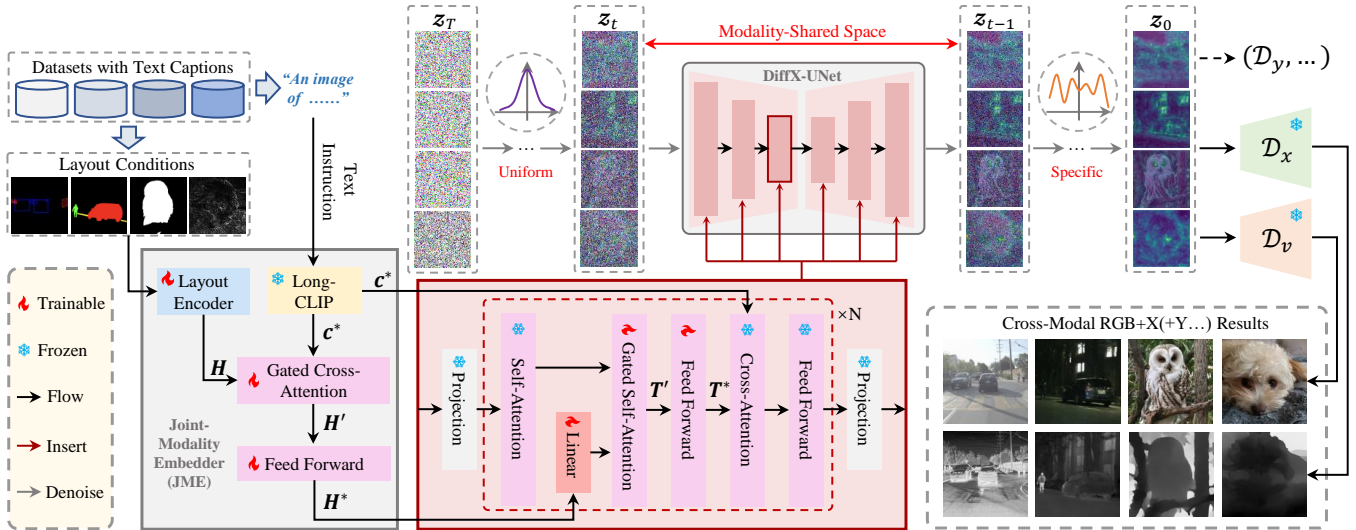


Figure 3: The workflow of our DiffX model for cross-modal generation. It performs the diffusion and denoising processes in the modality-shared space. Finally, the denoised feature z_0 is decoded into the “RGB+X(+Y)” images via multi-path decoders.

curate captions, especially in complex scenes. Therefore, in cases where the generated captions exhibit minimal errors, we conduct manual corrections to ensure the accuracy. However, instances of significant errors or ambiguous descriptions necessitate further corrections. Under such conditions, we utilize the GPT-4o model (Achiam et al. 2023) to rectify inaccurate information and provide additional descriptions.

By combining the capability of the LLaVA model with the manual correction and assistance of GPT-4o, the captioning process ensures fidelity and accuracy in describing the visual context in the cross-modal datasets. Examples of the data and prepared captions are shown in Figure 2 (b).

4 DiffX for Cross-Modal Generation

The workflow of our DiffX model is shown in Figure 3. The noisy latent z_T is randomly initialized, which is adopted for generating $z_{T-1}, z_{T-2}, \dots, z_0$ by our DiffX-UNet. The denoising process involves embedding the text captions and layout conditions for flexible user instruction.

In the following subsections, we first introduce the preliminaries on Latent Diffusion Model (LDM), and then we describe the workflow of our DiffX in detail.

4.1 Preliminaries on Latent Diffusion Model

Recently, LDM and its successor SD (Rombach et al. 2022) have pushed the boundaries of diffusion models by using a low-dimensional latent space. Inside LDM, a prior VAE is employed to extract the latent representation z of the ground-truth image I . Subsequently, the basic denoising model ϵ_θ , normally implemented as a UNet (Ronneberger, Fischer, and Brox 2015) with residual (He et al. 2016) and self-attention (Vaswani et al. 2017) blocks, is adopted to obtain the noise ϵ in the noisy latent z_t at time step t . The training objective can be represented as:

$$\min_{\boldsymbol{\theta}} \mathcal{L}_{\text{LDM}} = \mathbb{E}_{\boldsymbol{z}_t, \boldsymbol{\epsilon} \sim \mathcal{N}(\mathbf{0}, \mathbf{I}), t, \boldsymbol{c}} \left[\|\boldsymbol{\epsilon} - \boldsymbol{\epsilon}_{\boldsymbol{\vartheta}}(\boldsymbol{z}_t, t, \boldsymbol{c})\|_2^2 \right], \quad (1)$$

where c denotes the conditional input.

Following the training process, the denoising model ϵ_θ gradually generates $z_{T-1}, z_{T-2}, \dots, z_0$ from a randomly initialized noisy latent z_T . Finally, the decoder of VAE is employed to generate the target image I' based on z_0 .

4.2 Cross-Modal Modeling Formulation

In our DiffX model, we first obtain the joint-modality distribution by mapping the cross-modal images into the shared latent space. Specifically, during the forward process, the noising transition is conditioned on the joint modality $\mathbf{M} = \{m_1, m_2, \dots, m_N\}$, which can be expressed as:

$$q(\mathbf{z}_t, \mathbf{M} | \mathbf{z}_{t-1}) = q(\mathbf{z}_t | \mathbf{z}_{t-1}, \mathbf{M}) \prod_{i=1}^N q_i(\mathbf{m}_i). \quad (2)$$

Meanwhile, the reverse process can be regarded as the converse of the forward distributions, resulting in a joint distribution $p_{\theta}(z_{t-1}, \mathbf{M}|z_t)$ at time step t :

$$p_{\theta}(z_{t-1}, \mathbf{M}|z_t) \equiv p_{\theta}(z_{t-1}|z_t) \prod_{i=1}^N p_{\theta}(m_i|z_t), \quad (3)$$

where θ denotes the parameters of the DiffX model.

4.3 Multi-Path Variational AutoEncoder

As illustrated in Figure 4, the proposed MP-VAE is critical for our cross-modal generative task. In contrast to the conventional VAE used in LDM, our MP-VAE employs the input form of “RGB+X(+Y)” and output form of “RGB+X(+Y)”. Here, we take RGB+X modal encoding for illustration. In detail, the MP-VAE utilizes a single encoder \mathcal{E} to encode the input $\{\mathbf{I}_v, \mathbf{I}_x\}$ (denoted as $\{\mathbf{m}_1, \mathbf{m}_2\}$ in Eq. (2)) into the modality-shared latent representation z . The input images are processed through the separate convolutional layers, followed by element-wise addition before being fed to \mathcal{E} . Then, it incorporates parallel decoders \mathcal{D}_v and \mathcal{D}_x to generate the corresponding output $\{\mathbf{I}'_v, \mathbf{I}'_x\}$.

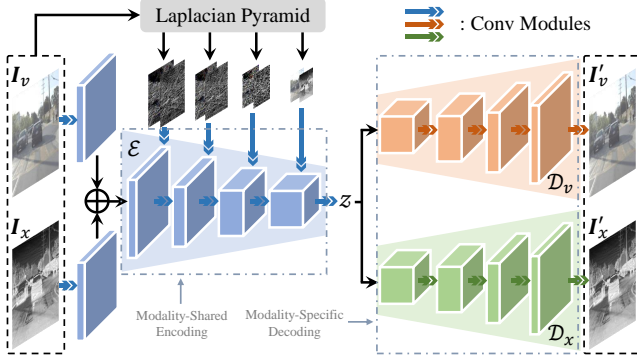


Figure 4: Workflow of our Multi-Path Variational AutoEncoder (MP-VAE). Here, the RGB+X modal encoding is employed for illustration. However, the framework is capable of supporting additional modal inputs and outputs.

In addition, we have observed that additional modality “X(+Y)” usually exhibits distinct contour edges and prominent object positions. To enhance the reconstruction ability of the MP-VAE, we apply a Laplacian Pyramid (LP) (Burt and Adelson 1987) to extract the high-frequency information from the input cross-modal image pairs. We adopt the Laplacian pyramid feature extraction strategy in the LPTN algorithm (Liang, Zeng, and Zhang 2021). Subsequently, the extracted features are embedded into the multi-scale layers of the encoder through cascaded convolutional layers, enabling a comprehensive enhancement at various frequencies.

During the inference phase of DiffX, the parallel decoders from the pre-trained MP-VAE are employed to generate the cross-modal “RGB+X(+Y)” images or more diverse modalities based on the denoised latent feature z_0 .

4.4 Joint-Modality Embedder

To establish a comprehensive connection between the layout (b/m) and the text (c), we propose the JME (\mathcal{J}_ω):

$$\mathbf{H}^*, \mathbf{c}^* = \mathcal{J}_\omega(b/m, c), \quad (4)$$

where \mathbf{H}^* is the text-aware layout feature, and \mathbf{c}^* is the caption feature. In detail, \mathcal{J}_ω consists of the layout encoder, Long-CLIP text encoder, a gated cross-attention layer, and a Feed Forward (FF) layer. The FF layer is a Multi-Layer Perception (MLP) with middle-dimensional expansion.

Layout Condition Embedding. 1) For the box-based layout, boxes b_i and labels l_i are embedded via Fourier mapping $\mathcal{F}(\cdot)$ (Tancik et al. 2020) and CLIP text encoder $f_{\text{clip}}(\cdot)$, respectively. Then, an MLP with parameters ϕ is used to encode them into grounding tokens:

$$\mathbf{h}_i = \text{MLP}_\phi([\mathcal{F}(b_i), f_{\text{clip}}(l_i)]); \mathbf{H} = [\mathbf{h}_1, \dots, \mathbf{h}_n], \quad (5)$$

where $[\cdot]$ denotes the feature concatenation. The representation \mathbf{H} , which contains a total of n embedded box features, is adopted as the layout conditional feature.

2) For the semantic mask layout represented by m , we utilize the the pre-trained ConvNeXt $_\psi$ model (Liu et al. 2022) to extract the in-depth semantic feature. Subsequently,

the position embedding \mathbf{p} is added, and an MLP with parameters φ is used to generate the layout feature:

$$\mathbf{H} = \text{MLP}_\varphi(\mathcal{R}(\text{ConvNeXt}_\psi(\mathbf{m})) + \mathbf{p}), \quad (6)$$

where \mathcal{R} denotes the process of reshaping and flattening the semantic feature into tokens.

Long-CLIP Caption Embedding. Text conditions c remain equally significant in cross-modal generation as they provide detailed image descriptions, including various aspects such as weather, environments, and transportation. Specifically, our task necessitates long text captions to describe the small objects and complex backgrounds in the cross-modal scene, as shown in Figure 2 (b). In our DiffX, we utilize the advanced Long-CLIP as the text encoder, which represents a significant improvement over its predecessor, CLIP, due to its ability to support text inputs of up to 248 tokens. In detail, each caption c is embedded into a sequence of text embeddings $\mathbf{c}^* = f_{\text{L-clip}}(\mathbf{c})$.

Gated Cross-Attention. Inside our \mathcal{J}_ω , the gated Cross-Attention (CA) layer is implemented to fuse the layout and text conditional features, which is formulated as follows:

$$\text{CA}(\mathbf{H}, \mathbf{c}^*) = \text{softmax} \left(\frac{W_q(\mathbf{H}) \cdot W_k(\mathbf{c}^*)^T}{\sqrt{d_k}} \right) \cdot W_v(\mathbf{c}^*), \quad (7)$$

where W_q , W_k , and W_v denote the linear transformations, and d_k denotes the dimension of $W_k(\mathbf{c}^*)$. Here, the CA layer derives query from layout condition \mathbf{H} , while deriving key and value from text condition \mathbf{c}^* .

In detail, a gated CA layer and an FF layer are sequentially implemented in \mathcal{J}_ω , which aim to generate the text-aware layout conditional feature \mathbf{H}^* :

$$\mathbf{H}' = \mathbf{H} + \lambda \cdot \tanh(\gamma_1) \cdot \text{CA}(\mathbf{H}, \mathbf{c}^*), \quad (8)$$

$$\mathbf{H}^* = \mathbf{H}' + \lambda \cdot \tanh(\gamma_2) \cdot \text{FF}(\mathbf{H}'), \quad (9)$$

where the hyperparameter λ plays a crucial role in balancing feature quality and controllability. Additionally, γ_1 and γ_2 are two adaptive learnable scalars inside the \tanh activation.

4.5 DiffX-UNet

As illustrated in Figure 3, DiffX-UNet serves as the basic model for the denoising process in the modality-shared latent space. It is composed of cascaded residual blocks and Spatial-Transformer blocks. The Spatial-Transformer block is the critical component of the DiffX-UNet, consisting of cascaded attention-based layers and FF layers. To enhance the training efficiency, pre-trained model weights from SD-v1-4 are initialized for the frozen layers.

The joint-modality feature \mathbf{H}^* embedded by \mathcal{J}_ω is fed into the gated Self-Attention (SA) layer within the Spatial-Transformer blocks, which acts as an adapter module to capture the cross-modal relationships. Similar to the gated CA layer, an FF layer is integrated after each gated SA layer to build the long-range interaction:

$$\mathbf{T}' = \mathbf{T} + \mu \cdot \tanh(\delta_1) \cdot \mathcal{T}(\text{SA}([\mathbf{T}, f_{\text{linear}}(\mathbf{H}^*)])), \quad (10)$$

$$\mathbf{T}^* = \mathbf{T}' + \mu \cdot \tanh(\delta_2) \cdot \text{FF}(\mathbf{T}'), \quad (11)$$

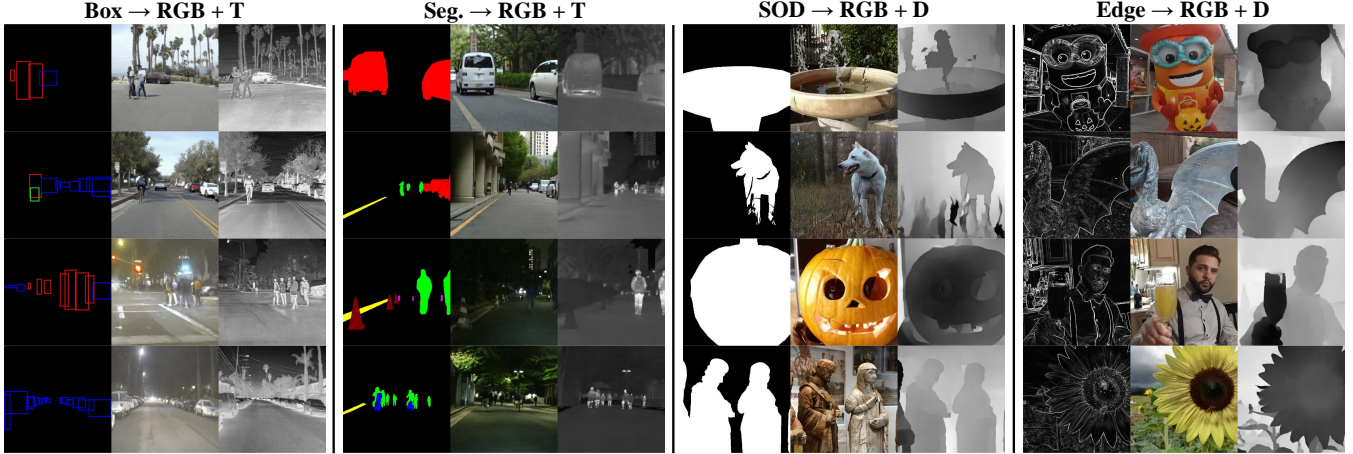


Figure 5: Qualitative results of cross-modal “RGB+X” generation by our DiffX. The synthesis resolution is fixed to 512×512 .

where $\mathcal{T}(\cdot)$ is a token selection operation that selects the visual token positions of \mathbf{T} . The hyperparameter μ adjusts the weights of the SA mechanism, whereas δ_1 and δ_2 are also two learnable scalars. For the trainable FF layers, we also add the scaling factors with the tanh activation.

Compared with the conventional Transformer blocks in SD, our Spatial-Transformer blocks integrate the iterative gated SA layers to adaptively embed the joint-modality layout feature \mathbf{H}^* . Moreover, the text condition \mathbf{c}^* embedded by Long-CLIP further enhances the long caption awareness.

4.6 Training & Inference

Training. Algorithm 1 shows the optimization process.

1) The training of MP-VAE is critical prior to the training of DiffX for cross-modal generation, where we encode the cross-modal images into the modality-shared latent space \mathbf{z} and conduct end-to-end reconstruction. The training objective of MP-VAE includes the MSE loss and perceptual loss (Johnson, Alahi, and Fei-Fei 2016):

$$\tilde{\mathcal{L}}_{\text{MP}} \triangleq \mathcal{L}_{\text{mse}}(\mathbf{M}, \widehat{\mathbf{M}}) + \sum_{i=1}^N \text{KL}(q_i(\mathbf{m}_i) \| p_{\theta}(\mathbf{m}_i | \mathbf{z})), \quad (12)$$

where the second term denotes the perceptual loss fitted with Kullback-Leibler (KL) divergence.

2) The training objective of our DiffX model, namely the latent denoising function, is formulated as:

$$\tilde{\mathcal{L}}_{\text{DiffX}} \triangleq \mathbb{E}_{\mathbf{q}}[\sum_{t>1} \|\mathbf{\epsilon} - \mathbf{\epsilon}_{\theta}(\mathbf{z}_t, t, \mathbf{c}^*, \mathbf{H}^*)\|_2^2], \quad (13)$$

where $t \sim \text{Uniform}\{1, \dots, T\}$ is sampled in each iteration. Then, the latent $\mathbf{z}_t \sim q(\mathbf{z}_t | \mathbf{z}_0, \mathbf{M})$ is initialized, which is fed into the DiffX model to predict the forward noise.

Inference. The difference in the sampling steps between our DiffX and conventional LDM is the multi-branch decoding by our MP-VAE. The main purpose is to estimate cross-modal images from features of the corresponding latent distributions inside the DiffX model.

5 Experiments

5.1 Cross-Modal Datasets

We conduct experiments on four “RGB+X(+Y+Z)” datasets for six cross-modal generative tasks. In detail, we adopt

Algorithm 1: Optimization process of DiffX.

STEP1: Training MP-VAE.

- 1: **While** training:
- 2: Forward: $\{\mathbf{I}'_v, \mathbf{I}'_x\} = \text{MP-VAE}(\{\mathbf{I}_v, \mathbf{I}_x\})$;
- 3: Minimize: $\tilde{\mathcal{L}}_{\text{MP}}$ formulated in Eq. (12);
- 4: Update: MP-VAE;
- 5: **End While.**

STEP2: Training DiffX (DiffX-UNet denoted as ϵ_{θ}).

- 6: Define: $\alpha_1, \alpha_2, \dots, \alpha_T$ (derived from $\beta_1, \beta_2, \dots, \beta_T$);
- 7: **While** training:
- 8: Forward: $\mathbf{z}_0 = \text{MP-Encoder}(\{\mathbf{I}_v, \mathbf{I}_x\})$;
- 9: Forward: \mathbf{c}^* and \mathbf{H}^* based on \mathbf{c} and \mathbf{b}/\mathbf{m} ;
- 10: Sample: $t \sim \text{Uniform}\{1, \dots, T\}$, $\mathbf{\epsilon} \sim \mathcal{N}(\mathbf{0}, \mathbf{I})$;
- 11: Calculate: $\mathbf{z}_t = \sqrt{\alpha_t} \mathbf{z}_0 + \sqrt{1 - \alpha_t} \mathbf{\epsilon}$;
- 12: Minimize: $\mathbb{E}_{\mathbf{z}_0, \mathbf{\epsilon}, t} [\|\mathbf{\epsilon} - \epsilon_{\theta}(\mathbf{z}_t, t, \mathbf{c}^*, \mathbf{H}^*)\|_2^2]$;
- 13: Update: Trainable modules of DiffX;
- 14: **End While.**

the clean-version FLIR dataset (F.A.Group 2019; Zhang et al. 2020) for “Box → RGB+T” task and the MFNet dataset (Ha et al. 2017) for “Segmentation (Seg.) maps → RGB+T” task. The COME15K dataset (Zhang et al. 2021) is adopted for “SOD → RGB+D”, “Edge → RGB+D”, and “SOD → RGB+D+Edge” tasks. Meanwhile, we utilize MCXFace dataset (George, Mohammadi, and Marcel 2022) for “3DDFA → RGB+NIR+SWIR+T” task on human face images, where the 3DDFA (Zhu et al. 2017) is the 3D face layout, while NIR and SWIR denote the infrared images across different wavelength bands.

5.2 Experimental Results and Comparison

Unified Cross-Modal Generation. As shown in Figure 5, we can see that DiffX is a unified framework for cross-modal generation under various layout conditions. The RGB+T generation benefits from its precise control over object positions and shapes. Meanwhile, it excels at RGB+D generation, generating highly realistic images with fine color and texture details. Most significantly, the generated X images

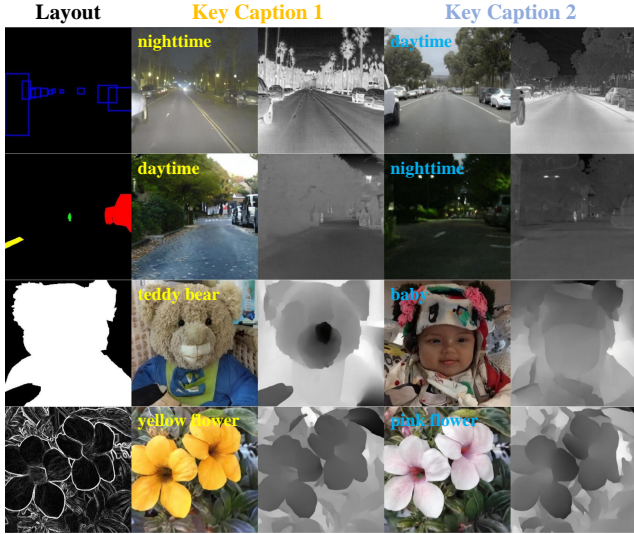


Figure 6: Diverse cross-modal generation by caption editing.

exhibit strong alignment with the RGB images, demonstrating its ability to generate coherent RGB+X image pairs.

Additionally, DiffX also enables the diverse cross-modal generation by editing the key captions, as shown in Figure 6. In traffic-scene RGB+T generation, the generated weather condition can be changed by modifying keywords like “daytime” and “nighttime”, which is critical in autonomous driving systems. For the natural RGB+D generation, we can change the categories and attributes of the generated objects by adjusting the captions while keeping their structural integrity and outlines. Therefore, it facilitates both creative manipulation and cross-modal image editing.

Comparison with Existing Models. To our knowledge, our DiffX is the first model for cross-modal generation. Although the baseline models were designed for RGB image generation, we can modify them to have dual outputs for comparison (modifications in appendix). Considering the model adaptability, we compare DiffX with the baselines in tasks of Seg. → RGB+T and Edge → RGB+D.

As shown in Figure 7, we can see that our DiffX significantly outperforms the baseline methods in qualitative results. The VQVAE (Van Den Oord, Vinyals et al. 2017) exhibits poor generative performance due to its unsuitability for multi-path outputs in end-to-end training. The VQGAN (Esser, Rombach, and Ommer 2021) and DDPM (Ho, Jain, and Abbeel 2020) can generate overall high-quality images but lack precision in capturing target objects and details. The modified GLIGEN (Li et al. 2023), which also performs diffusion training in a modality-shared latent space, yields superior results compared with other baseline models. However, it fails to generate accurate backgrounds in the nighttime scene despite using captions for guidance. It proves the effectiveness of employing Long-CLIP for caption embedding and JME for joint-modal connection.

On the other hand, we evaluate the generated image quality by LPIPS (Zhang et al. 2018) and FID (Heusel

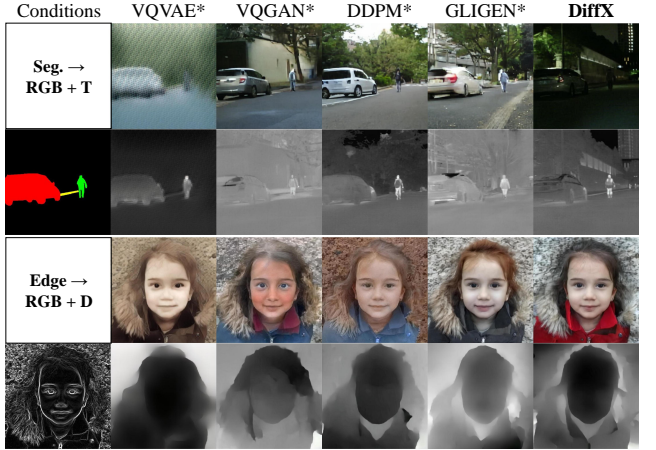


Figure 7: Qualitative comparison with the baseline models. The symbol * denotes the modified versions.

Table 1: Quantitative comparison with the baseline models.

Task	Model	LPIPS _{RGB → X} ↓	FID _{RGB → X} ↓	IoU↑	Acc↑	SSIM _x ↑
Seg. → RGB + T	VQVAE*	0.673 0.588	91.58 98.61	0.437	0.596	0.508
	VQGAN*	0.552 0.489	70.24 81.05	0.518	0.659	0.630
	DDPM*	0.535 0.457	71.53 78.69	0.535	0.672	0.617
	GLIGEN*	0.548 0.428	69.77 73.58	0.520	0.667	0.641
	DiffX	0.513 0.382	60.10 62.35	0.537	0.693	0.667
Task	Model	LPIPS _{RGB → X} ↓	FID _{RGB → X} ↓	S_α ↑	M ↓	SSIM _x ↑
Edge → RGB + D	VQVAE*	0.411 0.285	46.82 55.80	0.721	0.167	0.653
	VQGAN*	0.389 0.290	40.82 41.58	0.733	0.159	0.747
	DDPM*	0.255 0.208	26.79 34.18	0.751	0.140	0.768
	GLIGEN*	0.249 0.211	25.07 34.06	0.743	0.152	0.762
	DiffX	0.246 0.197	17.11 31.20	0.764	0.134	0.795

↑ / ↓ denotes that higher / lower values are better.

et al. 2017). Meanwhile, we adopt the pre-trained models in downstream tasks to evaluate the correspondence to the original layouts. We use EGFNet (Zhou et al. 2022) to test mean Intersection over Union (IoU) and mean Accuracy (Acc) on Seg. → RGB+T task, and use BBSNet (Fan et al. 2020) to test S-measure (S_α) (Fan et al. 2017) and Mean Absolute Error (M) scores on Edge → RGB+D task. Additionally, we employ the SSIM score (Wang et al. 2004) to evaluate the consistency of generated and ground-truth X images. The results in Table 1 demonstrate that our DiffX outperforms all baseline models in all metrics. Our impressive LPIPS and FID scores demonstrate the high-quality image generation by DiffX. Furthermore, the outstanding performance on downstream tasks highlights the effectiveness of DiffX in data augmentation for cross-modal vision tasks. Finally, the achieved SSIM scores on the X images (0.667 and 0.795 on the two tasks, respectively) illustrate the advantage of our approach for consistent layout-aware cross-modal generation.

Ablation Study. Firstly, we conduct the ablation study on the Laplacian Pyramid (LP) in our MP-VAE. Results in Table 2 show that the LP structure effectively improves

Table 2: Ablation study on Laplacian Pyramid (LP) in MP-VAE for cross-modal image reconstruction.

(↑)	Dataset	Source	MP-VAE w/o LP RGB	X	MP-VAE w/ LP RGB	X
PSNR	FLIR	RGB+T	29.04	29.77	29.25	30.89
	MFNet	RGB+T	30.59	30.96	31.45	32.86
	COME	RGB+D	30.09	34.19	30.15	35.73
SSIM	FLIR	RGB+T	0.785	0.719	0.792	0.737
	MFNet	RGB+T	0.788	0.845	0.800	0.919
	COME	RGB+D	0.729	0.958	0.749	0.974

Table 3: Quantitative comparison between the uni-modal DiffX_s and **cross-modal DiffX** on generated image quality.

(↓)	Task	DiffX _s RGB	X	DiffX RGB	X
LPIPS	Box → RGB+T	0.557	0.604	0.527	0.497
	Seg. → RGB+T	0.551	0.424	0.513	0.382
	SOD → RGB+D	0.718	0.489	0.579	0.305
	Edge → RGB+D	0.258	0.215	0.246	0.197
FID	Box → RGB+T	56.31	76.46	55.72	61.89
	Seg. → RGB+T	71.58	75.17	60.10	62.35
	SOD → RGB+D	71.23	80.54	51.59	52.83
	Edge → RGB+D	19.36	35.60	17.11	31.20

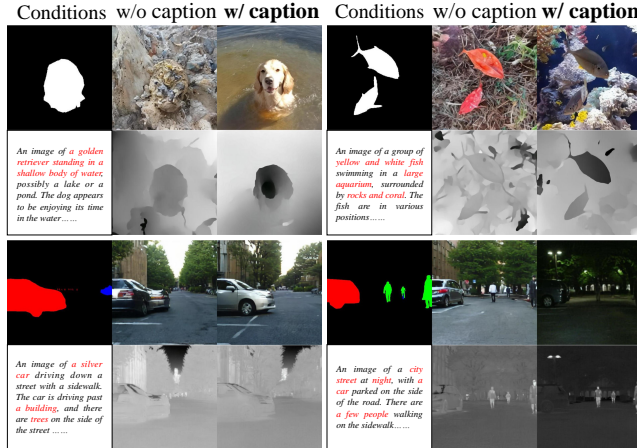


Figure 8: Impact of text captions in cross-modal generation.

the PSNR and SSIM, facilitating cross-modal reconstruction through frequency information incorporation.

Secondly, we aim to compare the uni-modal generation with the cross-modal RGB+X generation by DiffX. Therefore, we convert DiffX into a standard generative model (denoted as DiffX_s) to generate RGB and X separately. Quantitative comparison in Table 3 shows that the cross-modal results generated by DiffX exhibit better LPIPS and FID scores. This is because the diffusion and denoising training in modality-shared space can provide key complementary information for joint RGB+X image generation.

Thirdly, we conduct the ablation study on the impact of text captions on SOD → RGB+D and Seg. → RGB+T tasks. The qualitative comparison in Figure 8 shows that DiffX can effectively capture the crucial captions, while the variant model without caption embeddings generates broken or

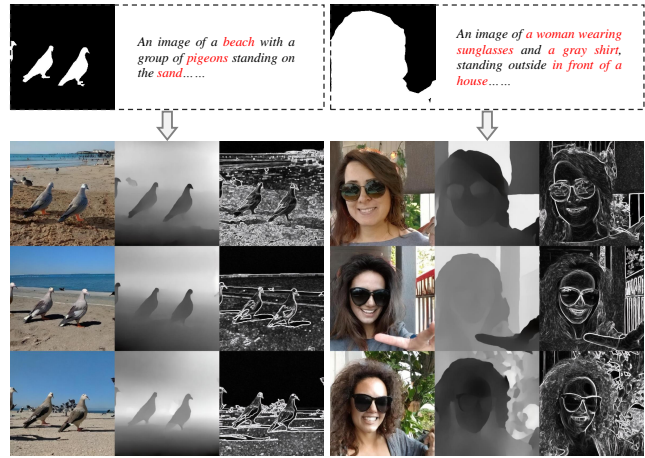


Figure 9: Adaptation to “SOD→RGB+D+Edge”.

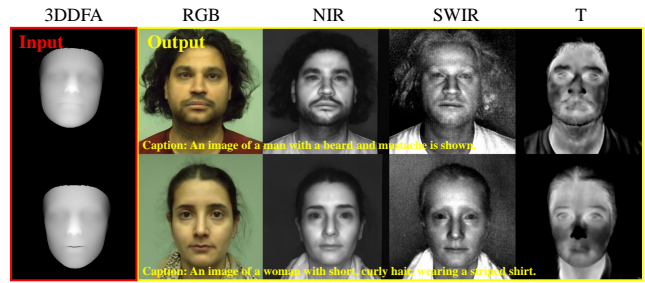


Figure 10: Adaptation to “3DDFA→RGB+NIR+SWIR+T”.

misaligned images, ultimately affecting the image quality. Therefore, it also necessitates incorporating Long-CLIP for embedding long text captions in cross-modal generation.

Adaptation to Diverse-Modal Generation. Given that DiffX’s can generate cross-modal “RGB+X” images, we also wonder *if we can apply this framework to robust, controllable, and versatile generation across diverse modalities?* Therefore, we also conduct experiments on COME15K and MCXFace datasets for “SOD → RGB+D+Edge” and “3DDFA → RGB+NIR+SWIR+T”, respectively.

The qualitative results are shown in Figure 9 and Figure 10, respectively. It is evident that the DiffX model can effectively adapt to diverse-modal “RGB+X+Y(+Z)” generation under various layout guidance. In addition, DiffX can accurately generate the images that align well with the provided text captions, where the RGB images also match the diverse-modal images effectively with the layout conditions. Therefore, DiffX is a standout choice for cohesive data augmentation across wide-range modalities. We also believe it can extend to cross-modal image-video generative modeling.

6 Conclusion

In this study, we introduce the DiffX model for cross-modal image generation under various layout conditions and text captions. The key innovation lies in its novel diffusion-based generative pipeline within a shared latent space across mul-

multiple modalities. Extensive experiments have demonstrated its robustness and adaptability in cross-modal generation. Meanwhile, the ablation study illustrates the effectiveness of the proposed modules in our DiffX model. Despite a slight increase in computational costs (less than 1%), it maintains superior efficiency when compared to training separate models for different modal generation. Moving forward, we aim to enhance our DiffX by enabling multiple-to-multiple generative modeling, allowing for the generation of unlimited modalities. Additionally, we also plan to incorporate diverse layout conditions and support simultaneous image-video generation for flexible user instruction.

References

Achiam, J.; Adler, S.; Agarwal, S.; Ahmad, L.; Akkaya, I.; Aleman, F. L.; Almeida, D.; Altenschmidt, J.; Altman, S.; Anadkat, S.; et al. 2023. Gpt-4 technical report. *arXiv preprint arXiv:2303.08774*.

Burt, P. J.; and Adelson, E. H. 1987. The Laplacian pyramid as a compact image code. In *Readings in computer vision*, 671–679. Elsevier.

Chen, C.; Ding, H.; Sisman, B.; Xu, Y.; Xie, O.; Yao, B.; Tran, S.; and Zeng, B. 2024. Diffusion models for multimodal generative modeling.

Esser, P.; Rombach, R.; and Ommer, B. 2021. Taming transformers for high-resolution image synthesis. In *Proceedings of the IEEE/CVF Conference on Computer Vision and Pattern Recognition*, 12873–12883.

F.A.Group. 2019. Flir thermal dataset for algorithm training. <https://www.flir.co.uk/oem/adas/adas-dataset-form/>.

Fan, D.-P.; Cheng, M.-M.; Liu, Y.; Li, T.; and Borji, A. 2017. Structure-measure: A new way to evaluate foreground maps. In *Proceedings of the IEEE international conference on computer vision*, 4548–4557.

Fan, D.-P.; Zhai, Y.; Borji, A.; Yang, J.; and Shao, L. 2020. BBS-Net: RGB-D Salient Object Detection with a Bifurcated Backbone Strategy Network. In *ECCV*.

Fang, Q.; Han, D.; and Wang, Z. 2021. Cross-modality fusion transformer for multispectral object detection. *arXiv preprint arXiv:2111.00273*.

George, A.; Mohammadi, A.; and Marcel, S. 2022. Prepended domain transformer: Heterogeneous face recognition without bells and whistles. *IEEE Transactions on Information Forensics and Security*, 18: 133–146.

Goodfellow, I. J.; Pouget-Abadie, J.; Mirza, M.; Xu, B.; Warde-Farley, D.; Ozair, S.; Courville, A.; and Bengio, Y. 2014. Generative Adversarial Networks. *arXiv:1406.2661*.

Ha, Q.; Watanabe, K.; Karasawa, T.; Ushiku, Y.; and Harada, T. 2017. MFNet: Towards real-time semantic segmentation for autonomous vehicles with multi-spectral scenes. In *2017 IEEE/RSJ International Conference on Intelligent Robots and Systems (IROS)*, 5108–5115. IEEE.

He, K.; Zhang, X.; Ren, S.; and Sun, J. 2016. Deep residual learning for image recognition. In *Proceedings of the IEEE conference on computer vision and pattern recognition*, 770–778.

Heusel, M.; Ramsauer, H.; Unterthiner, T.; Nessler, B.; and Hochreiter, S. 2017. Gans trained by a two time-scale update rule converge to a local nash equilibrium. *Advances in neural information processing systems*, 30.

Ho, J.; Jain, A.; and Abbeel, P. 2020. Denoising diffusion probabilistic models. *Advances in neural information processing systems*, 33: 6840–6851.

Johnson, J.; Alahi, A.; and Fei-Fei, L. 2016. Perceptual losses for real-time style transfer and super-resolution. In *Computer Vision–ECCV 2016: 14th European Conference, Amsterdam, The Netherlands, October 11–14, 2016, Proceedings, Part II* 14, 694–711. Springer.

Kingma, D. P.; and Welling, M. 2013. Auto-encoding variational bayes. *arXiv preprint arXiv:1312.6114*.

Li, X.; Qiu, K.; Chen, H.; Kuen, J.; Lin, Z.; Singh, R.; and Raj, B. 2024. ControlVAR: Exploring Controllable Visual Autoregressive Modeling. *arXiv preprint arXiv:2406.09750*.

Li, Y.; Liu, H.; Wu, Q.; Mu, F.; Yang, J.; Gao, J.; Li, C.; and Lee, Y. J. 2023. Glichen: Open-set grounded text-to-image generation. In *Proceedings of the IEEE/CVF Conference on Computer Vision and Pattern Recognition*, 22511–22521.

Liang, J.; Zeng, H.; and Zhang, L. 2021. High-resolution photorealistic image translation in real-time: A laplacian pyramid translation network. In *Proceedings of the IEEE/CVF Conference on Computer Vision and Pattern Recognition*, 9392–9400.

Liu, H.; Li, C.; Wu, Q.; and Lee, Y. J. 2024. Visual instruction tuning. *Advances in neural information processing systems*, 36.

Liu, Z.; Mao, H.; Wu, C.-Y.; Feichtenhofer, C.; Darrell, T.; and Xie, S. 2022. A convnet for the 2020s. In *Proceedings of the IEEE/CVF conference on computer vision and pattern recognition*, 11976–11986.

Ma, W.-D. K.; Lahiri, A.; Lewis, J.; Leung, T.; and Kleijn, W. B. 2024. Directed diffusion: Direct control of object placement through attention guidance. In *Proceedings of the AAAI Conference on Artificial Intelligence*, volume 38, 4098–4106.

Mizrahi, D.; Bachmann, R.; Kar, O.; Yeo, T.; Gao, M.; Dehghan, A.; and Zamir, A. 2024. 4m: Massively multimodal masked modeling. *Advances in Neural Information Processing Systems*, 36.

Nichol, A. Q.; and Dhariwal, P. 2021. Improved denoising diffusion probabilistic models. In *International conference on machine learning*, 8162–8171. PMLR.

Ramesh, A.; Dhariwal, P.; Nichol, A.; Chu, C.; and Chen, M. 2022. Hierarchical text-conditional image generation with clip latents. *arXiv preprint arXiv:2204.06125*, 1(2): 3.

Ramesh, A.; Pavlov, M.; Goh, G.; Gray, S.; Voss, C.; Radford, A.; Chen, M.; and Sutskever, I. 2021. Zero-shot text-to-image generation. In *International conference on machine learning*, 8821–8831. Pmlr.

Rombach, R.; Blattmann, A.; Lorenz, D.; Esser, P.; and Ommer, B. 2022. High-resolution image synthesis with latent

diffusion models. In *Proceedings of the IEEE/CVF conference on computer vision and pattern recognition*, 10684–10695.

Ronneberger, O.; Fischer, P.; and Brox, T. 2015. U-net: Convolutional networks for biomedical image segmentation. In *Medical image computing and computer-assisted intervention–MICCAI 2015: 18th international conference, Munich, Germany, October 5–9, 2015, proceedings, part III* 18, 234–241. Springer.

Ruan, L.; Ma, Y.; Yang, H.; He, H.; Liu, B.; Fu, J.; Yuan, N. J.; Jin, Q.; and Guo, B. 2023. Mm-diffusion: Learning multi-modal diffusion models for joint audio and video generation. In *Proceedings of the IEEE/CVF Conference on Computer Vision and Pattern Recognition*, 10219–10228.

Saharia, C.; Chan, W.; Saxena, S.; Li, L.; Whang, J.; Denton, E. L.; Ghasemipour, K.; Gontijo Lopes, R.; Karagol Ayan, B.; Salimans, T.; et al. 2022. Photorealistic text-to-image diffusion models with deep language understanding. *Advances in neural information processing systems*, 35: 36479–36494.

Shen, J.; Chen, Y.; Liu, Y.; Zuo, X.; Fan, H.; and Yang, W. 2024. ICAFusion: Iterative cross-attention guided feature fusion for multispectral object detection. *Pattern Recognition*, 145: 109913.

Sohl-Dickstein, J.; Weiss, E.; Maheswaranathan, N.; and Ganguli, S. 2015. Deep unsupervised learning using nonequilibrium thermodynamics. In *International conference on machine learning*, 2256–2265. PMLR.

Song, J.; Meng, C.; and Ermon, S. 2021. Denoising Diffusion Implicit Models. In *International Conference on Learning Representations*.

Tancik, M.; Srinivasan, P.; Mildenhall, B.; Fridovich-Keil, S.; Raghavan, N.; Singhal, U.; Ramamoorthi, R.; Barron, J.; and Ng, R. 2020. Fourier features let networks learn high frequency functions in low dimensional domains. *Advances in neural information processing systems*, 33: 7537–7547.

Tian, C.; Zhu, X.; Xiong, Y.; Wang, W.; Chen, Z.; Wang, W.; Chen, Y.; Lu, L.; Lu, T.; Zhou, J.; et al. 2024. Mm-interleaved: Interleaved image-text generative modeling via multi-modal feature synchronizer. *arXiv preprint arXiv:2401.10208*.

Van Den Oord, A.; Vinyals, O.; et al. 2017. Neural discrete representation learning. *Advances in neural information processing systems*, 30.

Vaswani, A.; Shazeer, N.; Parmar, N.; Uszkoreit, J.; Jones, L.; Gomez, A. N.; Kaiser, L.; and Polosukhin, I. 2017. Attention Is All You Need. *arXiv:1706.03762*.

Wang, X.; Darrell, T.; Rambhatla, S. S.; Girdhar, R.; and Misra, I. 2024. InstanceDiffusion: Instance-level Control for Image Generation.

Wang, Z.; Bovik, A. C.; Sheikh, H. R.; and Simoncelli, E. P. 2004. Image quality assessment: from error visibility to structural similarity. *IEEE transactions on image processing*, 13(4): 600–612.

Wu, Z.; Allibert, G.; Meriaudeau, F.; Ma, C.; and Demonceaux, C. 2023. Hidonet: Rgb-d salient object detection via hierarchical depth awareness. *IEEE Transactions on Image Processing*, 32: 2160–2173.

Xie, J.; Li, Y.; Huang, Y.; Liu, H.; Zhang, W.; Zheng, Y.; and Shou, M. Z. 2023. Boxdiff: Text-to-image synthesis with training-free box-constrained diffusion. In *Proceedings of the IEEE/CVF International Conference on Computer Vision*, 7452–7461.

Yang, B.; Luo, Y.; Chen, Z.; Wang, G.; Liang, X.; and Lin, L. 2023. Law-diffusion: Complex scene generation by diffusion with layouts. In *Proceedings of the IEEE/CVF International Conference on Computer Vision*, 22669–22679.

Zhang, B.; Zhang, P.; Dong, X.; Zang, Y.; and Wang, J. 2024. Long-clip: Unlocking the long-text capability of clip. *arXiv preprint arXiv:2403.15378*.

Zhang, H.; Fromont, E.; Lefevre, S.; and Avignon, B. 2020. Multispectral fusion for object detection with cyclic fuse-and-refine blocks. In *2020 IEEE International Conference on Image Processing (ICIP)*, 276–280. IEEE.

Zhang, J.; Fan, D.-P.; Dai, Y.; Yu, X.; Zhong, Y.; Barnes, N.; and Shao, L. 2021. RGB-D Saliency Detection via Cascaded Mutual Information Minimization. In *International Conference on Computer Vision (ICCV)*.

Zhang, R.; Isola, P.; Efros, A. A.; Shechtman, E.; and Wang, O. 2018. The unreasonable effectiveness of deep features as a perceptual metric. In *Proceedings of the IEEE conference on computer vision and pattern recognition*, 586–595.

Zhou, W.; Dong, S.; Xu, C.; and Qian, Y. 2022. Edge-aware guidance fusion network for rgb–thermal scene parsing. In *Proceedings of the AAAI conference on artificial intelligence*, volume 36, 3571–3579.

Zhu, X.; Liu, X.; Lei, Z.; and Li, S. Z. 2017. Face alignment in full pose range: A 3d total solution. *IEEE transactions on pattern analysis and machine intelligence*, 41(1): 78–92.